Phonon conduction in PbSe, PbTe, and $PbTe_{1-x}Se_x$ from first-principles calculations

Zhiting Tian,[1,*] Jivtesh Garg,[1] Keivan Esfarjani,[1] Takuma Shiga,[1,2] Junichiro Shiomi,[1,2] and Gang Chen[1,†]

[1]*Department of Mechanical Engineering, Massachusetts Institute of technology, Cambridge, Massachusetts 02139, USA*

[2]*Department of Mechanical Engineering, The University of Tokyo, Tokyo, 113-8656, Japan*

(Received 13 February 2012; published 14 May 2012)

We apply first-principles calculations to lead selenide (PbSe) and lead telluride (PbTe) and their alloys ($PbTe_{1-x}Se_x$), which are potentially good thermoelectric materials, to investigate their phonon transport properties. By accurately reproducing the lattice thermal conductivity, we validate the approaches adopted in this work. We, then, compare and contrast PbSe and PbTe, evaluate the importance of the optical phonons to lattice thermal conductivity, and estimate the impacts of nanostructuring and alloying on further reducing the lattice thermal conductivity. The results indicate that (1) the optical phonons are important not only because they directly comprise over 20% of the lattice thermal conductivity but also because they provide strong scattering channels for acoustic phonons, which is crucial for the low thermal conductivity; (2) nanostructures of less than ~10 nm are needed to reduce the lattice thermal conductivity for pure PbSe and PbTe; and (3) alloying should be a relatively effective way to reduce the lattice thermal conductivity.

DOI: 10.1103/PhysRevB.85.184303 PACS number(s): 63.20.kg, 63.20.Ry, 84.60.Rb, 71.15.Mb

I. INTRODUCTION

Thermoelectric materials are of great interest for their potential in converting heat into electricity.[1–5] The efficiency of thermoelectric power generators is determined by the dimensionless figure of merit zT ($zT = S^2\sigma T/k$, where S is the Seebeck coefficient, σ is the electrical conductivity, $S^2\sigma$ is the power factor, and k is the thermal conductivity). Semiconducting lead chalcogenides, such as PbSe and PbTe, are attractive thermoelectric materials for intermediate temperature (600–800 K) applications.[3] Significant efforts have been made to enhance the zT value of PbTe.[2–11] By introducing resonant states, Tl-doped p-type PbTe resulted in a high zT value of 1.5 at 773 K.[4] Nonresonant doping can also lead to $zT \sim 1.3$ around 700 K in K or Na-doped p-type PbTe.[6] Through band engineering to converge the valence bands, an extraordinary zT value of 1.8 at about 850 K was reported for doped $PbTe_{1-x}Se_x$ alloys.[7] Heremans *et al.*[8] observed the enhancement of the Seebeck coefficient in PbTe with nanograins. As the sister material of PbTe, PbSe has received much less attention although Se is more abundant and PbSe may offer an inexpensive alternative to PbTe, especially for high-temperature power generation. A recent calculation by Parker and Singh,[12] predicted that heavily doped PbSe may reach $zT \sim 2$ at 1000 K due to the flattening of the valence band. The experiments[13,14] later reported that the zT values could reach 1.2 and 1.3 at 850 K for heavily doped p-type and Al-doped n-type PbSe, respectively.

Past efforts in increasing the zT of PbTe and PbSe have mostly been based on improving the power factor $S^2\sigma$. Another approach to improve zT is to reduce the lattice thermal conductivity without substantially sacrificing the electronic properties. Previous studies[15–17] demonstrated the competence of the nanostructuring in suppressing the lattice thermal conductivity and thus improving zT. Most of the recent experimental studies on the strong reduction of the lattice thermal conductivity in nanostructured PbTe[9,10] emphasized the importance of dislocations, nanoscale precipitates, and strain, while pointing out that the mere presence of nanostructuring cannot sufficiently increase the phonon scattering. He *et al.*[11] found that not all nanostructures favorably scatter phonons. A necessary condition for the nanostructures to be effective in scattering phonons is to have their characteristic lengths, such as nanoparticle diameter and/or interparticle spacing, to be comparable or less than the phonon mean-free path (MFP). First-principles calculations on some thermoelectric materials show that phonons have a wide MFP distribution, and hence relatively large nanostructures can reduce their lattice thermal conductivity.[5,18,19] On the other hand, recent first-principles calculations have shown that the distribution is much narrower for PbTe,[20] and thus, further characterizations of the distributions and the associated detailed heat conduction of lead chalcogenides are important for better material design. For example, the extracted MFPs from our calculation can be combined with the Monte Carlo sampling of phonon-free paths[21] to predict the thermal conductivity of nanostructures of lead chalcogenides.

Besides nanostructuring, alloying may be another approach to reduce the lattice thermal conductivity. Previous experimental and theoretical studies on Si-Ge alloys[22–24] have found dramatic decrease in the lattice thermal conductivity from pure Si and Ge. There are still few reports on $PbTe_{1-x}Se_x$, and they only cover partial compositions ($x < 0.3$). Based on the limited experimental data on bulk PbSe-PbTe alloy,[25], p-type PbSe-PbTe alloy,[7,26] and PbSe-PbTe nanodot superlattice,[27] the reduction is mild compared to Si-Ge alloys. The first-principles calculation of the lattice thermal conductivity for PbSe-PbTe alloys over the whole composition range would allow us to better estimate the impacts of alloying.

Despite the high symmetric rocksalt structure of PbSe and PbTe, the lattice thermal conductivities reported in experiments were as low as 1.7–2.2 W/mK at 300 K.[3], [13,28–30] The first-principles calculations are useful to gain insight into the low heat conduction, with the capability of accurately capturing the transport properties of each phonon mode, including the optical modes. In most bulk materials, the optical phonons are ignored for the lattice thermal conductivity calculation.[31] For instance, the optical phonons comprise only 5% of the lattice thermal conductivity in bulk Si at

room temperature.[19,32–35] When the system size reaches the nanoscale, the optical phonons can contribute about 20%.[36] Another perspective to examine the importance of optical phonons is the acoustic-optical scattering, as described by Ward and Broido.[37] They removed optical phonons and observed an over three times increase in the lattice thermal conductivity for Si. The large anharmonicity of optical phonons was emphasized in PbTe to address the low thermal conductivity.[38]

In this work, we explore the detailed phonon transport properties in PbSe and PbTe to gain more guidance for the thermoelectric applications. We first calculate harmonic and anharmonic force constants from density functional perturbation theory (DFPT) calculations[39–41] The anharmonic phonon lifetimes are then obtained based on Fermi's golden rule. The total lattice thermal conductivity is determined under the relaxation time approximation by summing up the contribution from each mode. Our results are validated by comparing with the reported experimental data. We present detailed analysis and quantify contributions from different phonon modes to the thermal conductivity for both PbSe and PbTe and discuss the importance of optical phonons and the potential impacts of nanostructuring and alloying on further lattice thermal conductivity reduction in both material systems.

II. METHODOLOGY

Accurate interatomic force constants (IFCs) are crucial for the lattice thermal conductivity calculation. We adopt the DFPT approaches for both PbSe and PbTe. DFPT approaches have demonstrated unparalleled accuracy in reproducing the lattice thermal conductivity[22,42,43] and are sufficiently computationally affordable for the simple rocksalt structure with only two atoms in the primitive cell. More specifically, in our work, both the harmonic and anharmonic IFCs are obtained based on DFPT calculations implemented in the *Quantum Espresso* package.[44] In the ground-state calculations, the newly developed norm conserving fully relativistic pseudopotentials,[45] which incorporate the spin-orbit interaction (SOI) effect appropriately are chosen under the local density approximation (LDA) for electron exchange-correlation potential. Through the sensitivity study of the lattice thermal conductivity with SOI and without SOI, we find that for both PbSe and PbTe, SOI effect is important, and the fully relativistic pseudopotentials are necessary. For example, the phonon lifetimes of all modes are noticeably larger with SOI, which results in twice larger thermal conductivity with SOI than that without SOI at 300 K.

A. Harmonic properties

The harmonic IFCs are obtained using the primitive cell calculation of two atoms. In the self-consistent calculation of electronic properties, a Monkhorst-Pack $10 \times 10 \times 10$ mesh[46] is used to sample electronic states in the first Brillouin zone and an energy cutoff of 60 Ry (~816 eV) is used for the plane-wave expansion to ensure the force convergence. In the following DFPT calculation, a Monkhorst-Pack $4 \times 4 \times 4$**q**-mesh is used to calculate the dynamical matrix at each **q** grid, which, through inverse Fourier transform to real space, gives the harmonic IFCs. The harmonic IFCs allow computation of the dynamical matrix at any **q** point

$$D^{\alpha\beta}_{\eta\eta'}(\mathbf{q}) = \frac{1}{\sqrt{m_\eta m_{\eta'}}} \sum_{l'} \Phi^{\alpha\beta}_{0\eta,l'\eta'} e^{i\mathbf{q}\cdot\mathbf{R}_{l'}}, \tag{1}$$

where Φ is the harmonic IFC, m is the atomic mass, $\mathbf{R}_{l'}$ is the translation vector of the unit cell l', η specifies the ηth atom in the primitive cell, and α, β are Cartesian components. The eigenvalues of the dynamical matrix yield the phonon frequencies and the dispersion, from which the phonon group velocities can be calculated.

B. Anharmonic properties

There are two approaches to calculate the anharmonic IFCs in the reciprocal space. The results from both approaches are equivalent. One approach is based on $2n+1$ theorem[47,48] that assumes the third-order IFCs can be obtained from the first-order wave function. It is computationally effective since it does not involve the supercell calculation but relatively complicated to implement. The other approach is to calculate the third-order IFCs from the second-order IFCs using the finite difference method, which is computationally more expensive but simpler to implement. We use the latter approach in this study.

The third-order derivatives are determined by taking the derivative of the second-order IFCs through a central difference scheme as below:

$$\begin{aligned}\Psi^{\alpha\beta\gamma}_{0\eta,l'\eta',l''\eta''} &= \frac{\partial^3 V}{\partial u^\alpha_{0\eta}\partial u^\beta_{l'\eta'}\partial u^\gamma_{l''\eta''}} \\ &= \frac{\frac{\partial^2 V}{\partial u^\beta_{l'\eta'}\partial u^\gamma_{l''\eta''}}\Big|_{u^\alpha_{0\eta}} - \frac{\partial^2 V}{\partial u^\beta_{l'\eta'}\partial u^\gamma_{l''\eta''}}\Big|_{-u^\alpha_{0\eta}}}{2u^\alpha_{0\eta}} \\ &= \frac{\Phi^{\beta\gamma}_{l'\eta',l''\eta''}\big|_{u^\alpha_{0\eta}} - \Phi^{\beta\gamma}_{l'\eta',l''\eta''}\big|_{-u^\alpha_{0\eta}}}{2u^\alpha_{0\eta}},\end{aligned} \tag{2}$$

where V is the interatomic potential. We first perform the Γ point phonon calculation in a supercell to generate the harmonic IFCs for two different atomic configurations, namely, involving displacement of an atom along positive and negative Cartesian directions around the equilibrium position. All the required cubic IFCs are obtained by sequentially changing the atom displaced to be any of the atoms in the primitive cell. To ensure the accuracy of the cubic IFCs, we test three values of displacements. We use a Monkhorst-Pack $4 \times 4 \times 4$ mesh[46] to sample electronic states with the same energy cutoff of 60 Ry (~816 eV).

The cubic IFCs are needed to compute the three-phonon scattering matrix elements, which measure the strength of the scattering events and are given by

$$\begin{aligned}&V_3(\mathbf{q}s,\mathbf{q}'s',\mathbf{q}''s'') \\ &= \left(\frac{\hbar}{8N_0\omega(\mathbf{q}s)\omega(\mathbf{q}'s')\omega(\mathbf{q}''s'')}\right)^{1/2} \sum_\eta \sum_{l'\eta'} \sum_{l''\eta''} \sum_{\alpha\beta\gamma} \\ &\times \Psi^{\alpha\beta\gamma}_{0\eta,l'\eta',l''\eta''} e^{i\mathbf{q}'\cdot\mathbf{R}_{l'}} e^{i\mathbf{q}''\cdot\mathbf{R}_{l''}} \frac{e^\alpha_\eta(\mathbf{q}s) e^\beta_{\eta'}(\mathbf{q}'s') e^\gamma_{\eta''}(\mathbf{q}''s'')}{\sqrt{m_\eta m_{\eta'} m_{\eta''}}},\end{aligned} \tag{3}$$

where $\hbar$ is the Planck constant divided by 2π, N_0 is the total number of modes in the first Brillouin zone, and s denotes different polarizations. By applying Fermi's golden rule to the cubic Hamiltonian,[49–52] the phonon lifetimes $\tau_{\mathbf{q}s}$ due to the normal and umklapp three-phonon scattering processes can be expressed as

$$\frac{1}{\tau_{\mathbf{q}s}} = 2\Gamma_{\mathbf{q}s} = \pi \sum_{\mathbf{q}'s'} \sum_{s} |V_3(\mathbf{q}s,\mathbf{q}'s',\mathbf{q}''s'')|^2 \times [2(n_{\mathbf{q}'s'} - n_{\mathbf{q}''s''})\delta(\omega(\mathbf{q}s) + \omega(\mathbf{q}'s') - \omega(\mathbf{q}''s'')) + (1 + n_{\mathbf{q}'s'} + n_{\mathbf{q}''s''})\delta(\omega(\mathbf{q}s) - \omega(\mathbf{q}'s') - \omega(\mathbf{q}''s''))], \tag{4}$$

where $n_{\mathbf{q}s}$ is the Bose-Einstein distribution $n_{\mathbf{q}s} = 1/(e^{\hbar\omega_{\mathbf{q}s}/k_BT} - 1)$. The conservation of momentum requires $\mathbf{q} + \mathbf{q}' + \mathbf{q}'' = \mathbf{G}$, given $\mathbf{G}$ as the reciprocal lattice vector, while $\mathbf{G} = 0$ results in the normal process and $\mathbf{G} \neq 0$ relates to the umklapp process. The choices of $\mathbf{q}''$ are limited by $\mathbf{q}$ and $\mathbf{q}'$, thus the summation involves only $\mathbf{q}'$.

C. Lattice thermal conductivity

We compute the lattice thermal conductivity based on the relaxation time approximation using the well-known formula

$$\kappa = \frac{1}{3\Omega N_0} \sum_{\mathbf{q}s} \mathrm{v}^2_{\mathbf{q}s} \tau_{\mathbf{q}s} \hbar\omega_{\mathbf{q}s} \frac{\partial n_{\mathbf{q}s}}{\partial T}, \tag{5}$$

where Ω is the volume of the unit cell and $\mathrm{v}_{\mathbf{q}s}$ is the amplitude of group velocity. We use a $30 \times 30 \times 30$ $\mathbf{q}$-mesh within the first Brillouin zone to ensure the convergence. Comparing the total value with the experimental data serves as a validation of our calculations.

More importantly, decomposition of the total lattice thermal conductivity into each mode allows us to account for the contributions from phonons with different MFPs and polarizations, which provide insights into the thermoelectric applications. The phonon MFP for each mode is defined as

$$\Lambda_{\mathbf{q}s} = \mathrm{v}_{\mathbf{q}s} \tau_{\mathbf{q}s}. \tag{6}$$

One way to quantify the contribution from phonons with various MFPs is to evaluate the thermal conductivity accumulation with respect to MFPs as described in Refs. 32 and 53. By summing the thermal conductivity contribution of modes with MFPs up to Λ, the cumulative thermal conductivity can be determined as follows:

$$\kappa(\Lambda) = \frac{1}{3\Omega N_0} \sum_{\mathbf{q}s}^{\Lambda_{\mathbf{q}s} < \Lambda} \mathrm{v}_{\mathbf{q}s} \Lambda_{\mathbf{q}s} \hbar\omega_{\mathbf{q}s} \frac{\partial n_{\mathbf{q}s}}{\partial T}. \tag{7}$$

To separate the contribution among different polarizations, we simply sum the thermal conductivity of the modes with certain polarization s as

$$\kappa_s = \frac{1}{3\Omega N_0} \sum_{\mathbf{q}} \mathrm{v}^2_{\mathbf{q}s} \tau_{\mathbf{q}s} \hbar\omega_{\mathbf{q}s} \frac{\partial n_{\mathbf{q}s}}{\partial T}. \tag{8}$$

D. Alloy modeling

To take into account the alloy effects, we use the virtual crystal approach, first introduced by Abeles,[23] where the disordered crystal is replaced with an ordered one of the average lattice parameter, atomic mass, and force constants according to the composition. The mass disorder and anharmonicity are both treated as perturbations. Garg *et al.*[22] has applied this approach to Si-Ge alloys using the force constants from DFPT and achieved excellent agreement with the experimental data.[23,24]

The effective phonon scattering rate is defined as the sum of the scattering rate due to mass disorder and anharmonicity:

$$\frac{1}{\tau_{\mathbf{q}s}} = \frac{1}{\tau^m_{\mathbf{q}s}} + \frac{1}{\tau^{p-p}_{\mathbf{q}s}}. \tag{9}$$

While the anharmonic phonon lifetimes $\tau^{p-p}_{\mathbf{q}s}$ are calculated in the same way as the pure cases except for different input parameters, the harmonic phonon lifetimes due to mass disorder follow eq. (12) in Ref. 54 as below

$$\frac{1}{\tau^m_{\mathbf{q}s}} = \frac{\pi}{2N} \omega^2_{\mathbf{q}s} \sum_{\mathbf{q}'s'} \delta(\omega_{\mathbf{q}s} - \omega_{\mathbf{q}'s'}) \sum_{\sigma} g_2(\sigma) |\mathrm{e}^*_{\mathbf{q}'s'}(\sigma) \cdot \mathrm{e}_{\mathbf{q}s}(\sigma)|^2, \tag{10}$$

where $\mathbf{e}$ is the polarization vector, $g_2(\sigma) = \sum_i f_i(\sigma)[1 - m_i(\sigma)/\overline{m_i}(\sigma)]^2$, $f_i(\sigma)$, and $m_i(\sigma)$ are the concentration and the atomic mass of ith isotope of the σ atom.

III. RESULTS AND DISCUSSION

A. Comparison with experimental results

Figure 1 shows the phonon dispersion relations of PbSe and PbTe along the high symmetry lines within the first Brillouin zone of the primitive cell with two atoms. There are six polarizations: two transverse acoustic (TA), one longitudinal acoustic (LA), two transverse optical (TO), and one longitudinal optical (LO) modes. The disperion of PbSe agrees reasonably well with the experimental results.[55] The splitting of LO and TO at Γ point, which depends on the Born effective charges and dielectric constants, agrees with that in the experiment. The dispersion of PbTe matches well with the experiments[56] except for the LO branch. The discrepancy at Γ point comes from the difference in the Born effective charges. By setting the Born effective charge to the value obtained in the experiment (6.5e), the dispersion meets the experimental data, while all other modes and the total thermal conductivity change by less than 1%. It has also been claimed in previous work[18,20] that the inclusion of the LO-TO splitting has only negligible effects. For better comparison in terms of the actual frequency range, we use the tuned Born effective charge for the latter discussions.

Although the frequency of the TO mode at the zone center matches perfectly with the experimental value measured at room temperature, some uncerntainties exist in the calculation of this specific mode. As found in previous studies, the TO mode at the Γ point is soft and directly relates to the ferroelectric ground state.[57,58] The ferroelectric mode is difficult to calculate accurately due to its strong tempearture and volume dependences, and different pseudopotentials and lattice constants lead to different frequencies.[57–59] However, since we focus on the integrated properties of all the phonon modes, the discrepancy of single mode or few modes near the

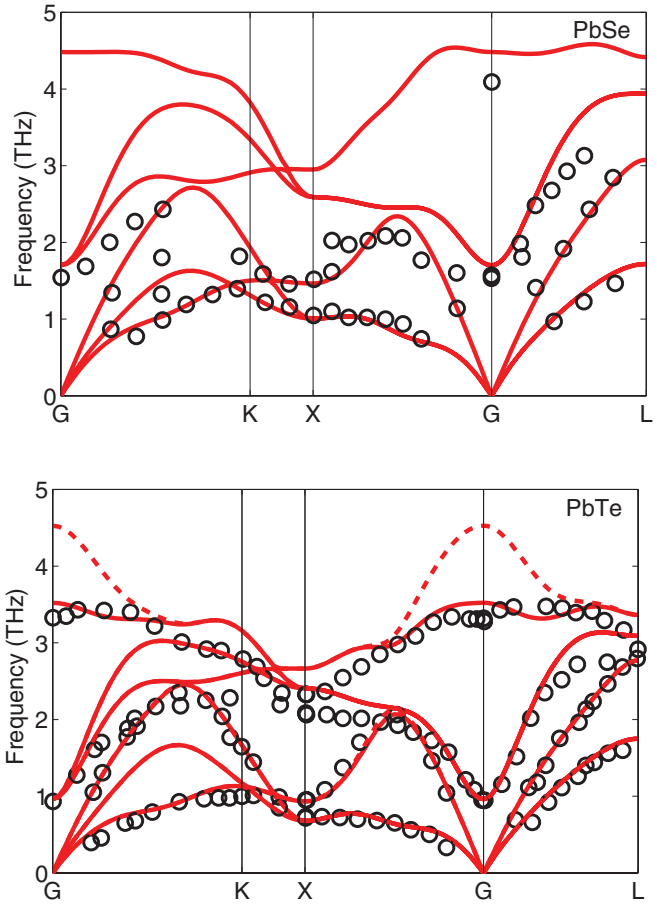

FIG. 1. (Color online) Phonon dispersion for PbSe and PbTe: red lines–calculated results and black dots—experimental results (Refs. 55 and 56).

zone center with very small or even zero group velocity does not make any noticeable change to our conclusions.

The dispersion relations of PbSe and PbTe are similar but do not scale with the total primitive cell mass ratio because they have one element Pb in common. Although the frequencies of the optical modes of PbTe drop significantly compared to those of PbSe, the differences between the acoustic modes, especially the TA modes, are much smaller.

We compare the calculated lattice thermal conductivities with experimental results in Fig. 2. For both PbSe and PbTe, the calculations achieve decent agreement with experimental values.[29,30] The small discrepancies of PbSe between 300 and 400 K might come from the impurity or defects scattering in the experimental sample, which becomes inferior to three-phonon scattering at higher temperatures. Above 400 K, the calculated results lie on top of the experimental data. The agreement for PbTe in the whole temperature range is excellent. The good representation bears out the accuracy of our approach, and the validity of the relaxation time approximation, and supports our following discussions.

B. Comparison between PbSe and PbTe

The calculated lattice thermal conductivity of PbSe is 11% higher than that of PbTe at temperatures of 300–700 K. The atomic masses of Pb, Se, and Te are 207.2, 78.96, and 127.6,

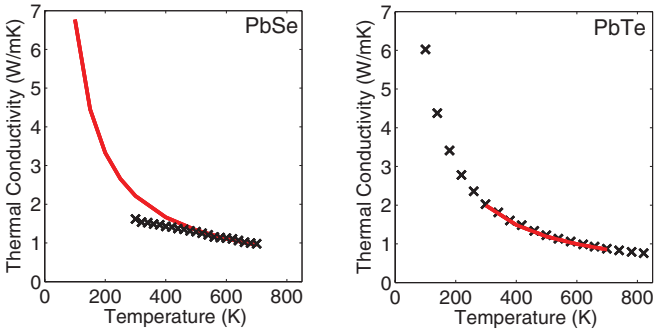

FIG. 2. (Color online) Temperature-dependent lattice thermal conductivity of PbSe and PbTe, red lines: calculated results; black crosses: experimental data (Refs. 29 and 30).

respectively. Se is about 40% lighter than Te, but due to the heavy mass of Pb, the mass difference for PbTe and PbSe is only 17%. At the first glance, the mass difference seems to fully explain the thermal conductivity difference. Yet how the mass difference actually leads to the variance in different quantities is far from the simple deduction, as we will show below.

We show the phonon lifetimes in Fig. 3. In the low-frequency range, the lifetimes exhibit ω^{-2} dependence, in agreement with Klemens' prediction.[60] The trends of the lifetimes with respect to frequencies are similar for PbSe and PbTe. For most of the TA modes, the lifetimes of PbSe are substantially larger than those of PbTe, while for LA and optical modes, the lifetimes of PbSe are not necessarily higher. This is a nontrivial observation since the anharmonicity of PbSe were normally expected to be larger due to the larger average Grüneisen parameter reported from experiments.[28] For optical modes, the lifetimes of PbTe are obviously larger.

With heavier mass, PbTe was anticipated to have smaller group velocities in general. Nevertheless, Fig. 4 shows that for TA modes, the group velocities of PbSe and PbTe are

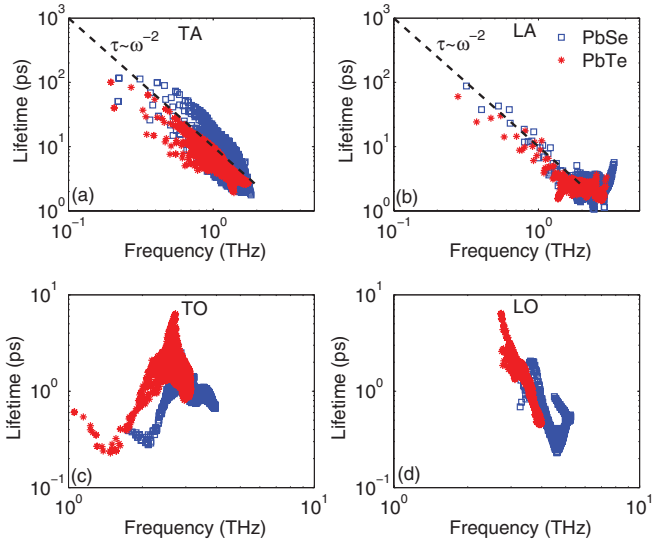

FIG. 3. (Color online) Frequency-dependent phonon lifetimes of PbSe (squares) and PbTe (crosses) at 300 K: (a) TA, (b) LA, (c) TO, and (d) LO.

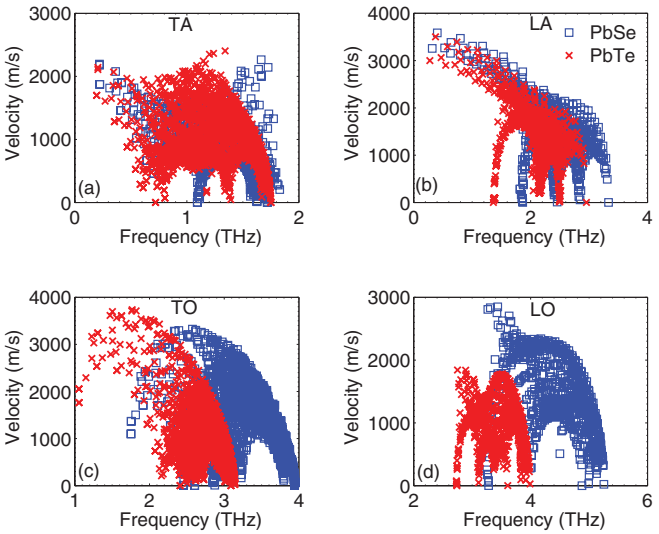

FIG. 4. (Color online) Frequency-dependent phonon group velocities of PbSe (squares) and PbTe (crosses) at 300 K: (a) TA, (b) LA, (c) TO, and (d) LO.

almost the same because of the closely matched acoustic dispersions. Noticeably, these TA modes are fairly soft with maximum value around 2000 m/s. In terms of the LA modes, the group velocities of PbSe are moderately higher. Between 1 and 2 THz, several TO modes of PbTe possess exceptionally high group velocities (>3500 m/s) and even higher than the TO modes of PbSe. For LO modes, the group velocities of PbTe are perceptibly smaller than those of PbSe.

Integrating the transport properties over the entire first Brillouin zone, we can obtain the polarization dependent thermal conductivities as shown in Fig. 5. Remarkably, over a wide temperature range of 300 to 700 K, the three acoustic branches contribute equally, and three optical branches contribute almost evenly to the thermal conductivity of PbTe. In the case of PbSe, by contrast, the contribution among acoustic and among optical modes are all distinguishable.

Considering all the differences in phonon frequencies, lifetimes, and group velocities, it is impossible to identify the decisive one source of the differences between PbTe and PbSe, despite the simple mass difference argument.

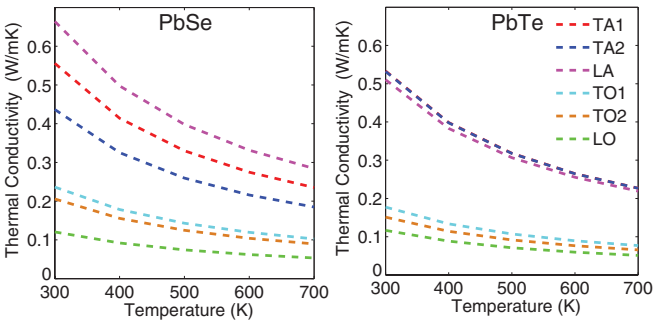

FIG. 5. (Color online) Thermal conductivity from different polarizations (TA1, TA2, LA, TO1, TO2, and LO) versus temperature for PbSe and PbTe.

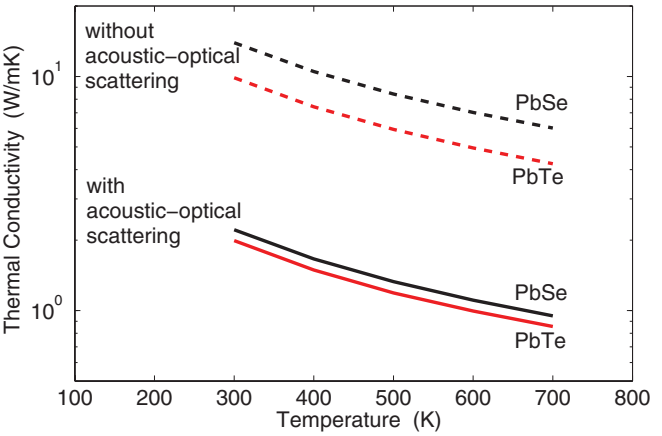

FIG. 6. (Color online) Temperature dependence of lattice thermal conductivity without and with acoustic-optical scattering: PbSe (black dashed lines), PbTe [red (medium gray) dashed lines].

C. The importance of optical phonons

The normalized optical phonon contributions can be calculated by adding the TO and LO modes together. For the whole temperature range considered (300–700 K), the contributions of optical phonons remain about 25% for PbSe and 22% for PbTe. These findings are rather surprising especially considering the simple rocksalt crystal structures of these two materials and the fact that only half of the modes are optical phonons. Our calculations demonstrate that optical phonons are not always negligible even in simple crystalline bulk materials.

Moreover, optical phonons provide important scattering channels for acoustic phonons and are essential for the low thermal conductivity of PbSe and PbTe. By removing the acoustic-optical scattering, the thermal conductivity of PbSe/PbTe increases dramatically by a factor of six/five over the entire temperature range investigated here (300 to 700 K) as shown in Fig. 6. This difference is about twice larger than that of Si.[37] Due to the softening of the optical phonons, the

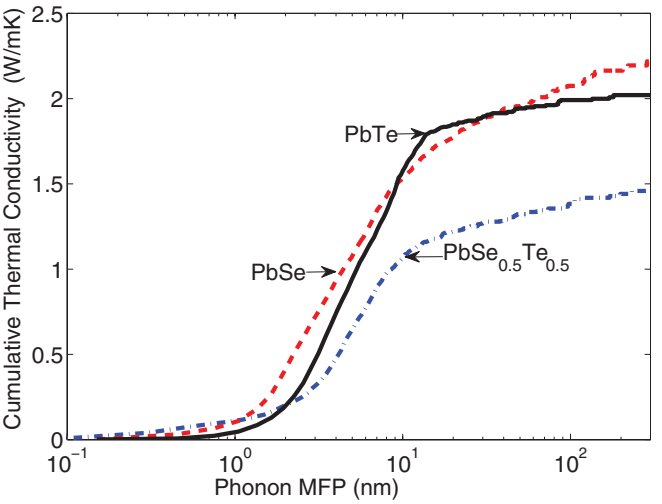

FIG. 7. (Color online) Cumulative thermal conductivity with respect to phonon MFP at 300 K for PbSe (red dashed line), PbTe (black solid line), and $PbTe_{0.5}Se_{0.5}$ (blue dotted line).

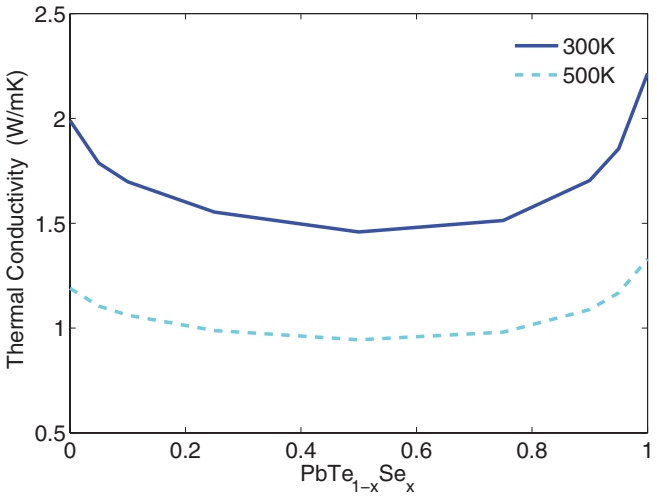

FIG. 8. (Color online) Composition dependence of the lattice thermal conductivity in $PbTe_{1-x}Se_x$ at 300 K (solid line) and 500 K (dashed line).

LA and TO phonons are strongly coupled, as observed in PbTe by Delaire *et al.*[38] in the experiment and by Shiga *et al.* in the calculation,[20] and help lower the lattice thermal conductivity.

D. The potential impacts of nanostructuring

The cumulative thermal conductivity with respect to phonon MFPs at 500 K is shown in Fig. 7. The total accumulation for PbSe keeps increasing as MFPs increases, while the accumulation for PbTe gradually approaches plateau after MFPs reach 10 nm. Phonons with MFPs smaller than 10 nm comprise around 80% of the lattice thermal conductivity for PbSe and about 90% for PbTe. In other words, even if the interface backscattered all the ballistic phonons, the nanostructuring with length scale 10 nm would only potentially reduce the thermal conductivity by 20% for PbSe and 10% for PbTe at the most. Therefore, to significantly reduce the lattice thermal conductivity in these materials, nanostructures with characteristic length smaller than 10 nm are required. Therefore, smaller inhomogeneities and alloying might be more effective in reducing the lattice thermal conductivity.

E. The potential impacts of PbSe-PbTe alloying

We plot the lattice thermal conductivity of different composition of $PbTe_{1-x}Se_x$ alloy in Fig. 8. At $x = 0.5$, we obtain a maximum decrease of 30% (1.46 W/mK) compared to the average lattice thermal conductivity of PbSe and PbTe (2.1 W/mK) at 300 K. There is no sharp decrease feature in the dilute alloy limit as reported in Si-Ge alloy[22] due to the small difference in acoustic impedance between PbSe and PbTe. As temperature increases, the phonon-phonon scattering becomes dominant, and the influence from alloy scattering becomes less important. Therefore, comparing 300 K with 500 K, the reduction of lattice thermal conductivity is slighter at 500 K.

The MFP accumulation of $PbTe_{0.5}Se_{0.5}$ is plotted in Fig. 7. The phonons with high frequencies and short MFPs are strongly scattered by mass disorder, while the phonons with small frequencies and long MFPs are much less influenced. This leads to redistribution among different MFPs and consequently the shift in the accumulation curve. Because the accumulation curve of $PbTe_{0.5}Se_{0.5}$ is considerably flat above 10 nm, similar to PbSe and PbTe, nanostructuring on alloys could not push down lattice thermal conductivity by a significant amount.

Taking into account the practical difficulty in introducing nanostructures at the scale of 10 nm and the potential reduction in the lattice thermal conductivity, the simple alloying approach is more promising in reducing the lattice thermal conductivity.

IV. CONCLUSIONS

We perform first-principles calculations to detail the spectral phonon transport properties of PbSe and PbTe. We first extract harmonic and anharmonic force constants from DFPT calculations within a supercell. We then extract the phonon lifetimes based on Fermi's golden rule and compute the thermal conductivity under the relaxation time approximation. The total lattice thermal conductivities quantitatively agree with the experimental results. Comparison of mode-dependent properties between PbSe and PbTe suggests that the transport properties of these two sister materials are similar in principle but different in specifics. The optical phonons not only directly contribute a considerable amount to the total lattice thermal conductivity of bulk PbSe and PbTe but also serve as important scattering channels for acoustic phonons. Both PbSe and PbTe possess very close lattice thermal conductivities, which is attractive for thermoelectric applications. Nanostructuring, however, would be difficult to further reduce the lattice thermal conductivity unless their characteristic lengths are reduced to less than 10 nm. Alloying, on the other hand, has advantages over nanostructuring in reducing the lattice thermal conductivity. The parallel studies of these two materials provide insights into the phonon properties and may help design better thermoelectric materials.

ACKNOWLEDGMENTS

This material is based upon work supported as part of the S3TEC, an Energy Frontier Research Center funded by the US Department of Energy, Office of Science, Office of Basic Energy Sciences under Award No. DE-FG02-09ER46577 (grant number). This research was supported in part by the National Science Foundation through TeraGrid resources provided by Ranger.

*zhiting@mit.edu
†gchen2@mit.edu

[1] H. J. Goldsmid, *Introduction to Thermoelectricity* (Springer, Berlin, 2009).
[2] G. J. Snyder and E. S. Toberer, Nat. Mater. **7**, 105 (2008).
[3] J. R. Sootsman, D. Y. Chung, and M. G. Kanatzidis, Angew. Chem. Int. Ed. **48**, 8616 (2009).
[4] J. P. Heremans, V. Jovovic, E. S. Toberer, A. Saramat, K. Kurosaki, A. Charoenphakdee, S. Yamanaka, and G. J. Snyder, Science **321**, 554 (2008).

[5]M. Zebarjadi, K. Esfarjani, M. S. Dresselhaus, Z. F. Ren, and G. Chen, Energy Environ. Sci. **5**, 5147 (2012).
[6]J. Androulakis, I. Todorov, D. Y. Chung, S. Ballikaya, G. Y. Wang, C. Uher, and M. Kanatzidis, Phys. Rev. B **82**, 115209 (2010).
[7]Y. Z. Pei, X. Y. Shi, A. LaLonde, H. Huang, L. D. Chen, and G. J. Snyder, Nature **473**, 66 (2011).
[8]J. P. Heremans, C. M. Thrush, and D. T. Morelli, Phys. Rev. B **70**, 115334 (2004).
[9]J. He, S. N. Girard, M. G. Kanatzidis, and V. P. Dravid, Adv. Funct. Mater. **20**, 764 (2010).
[10]J. He, J. R. Sootsman, S. N. Girard, J. C. Zheng, J. G. Wen, Y. M. Zhu, M. G. Kanatzidis, and V. P. Dravid, J. Am. Chem. Soc. **132**, 8669, (2010).
[11]J. Q. He, J. Androulakis, M. G. Kanatzidis, and V. P. Dravid, Nano Lett. **12**, 343 (2012).
[12]D. Parker and D. J. Singh, Phys. Rev. B **82**, 035204 (2010).
[13]H. Wang, Y. Z. Pei, A. D. LaLonde, and G. J. Snyder, Adv. Mater. **23**, 1366 (2011).
[14]Q. Y. Zhang, H. Wang, W. S. Liu, H. Z. Wang, B. Yu, Q. Zhang, Z. T. Tian, G. Ni, S. Lee, K. Esfarjani, G. Chen, and Z. F. Ren, Energy Environ. Sci. **5**, 5246 (2012).
[15]B. Poudel, Q. Hao, Y. Ma, Y. Lan, A. Minnich, B. Yu, X. Yan, D. Wang, A. Muto, D. Vashaee, X. Chen, J. Liu, M. S. Dresselhaus, G. Chen, and Z. Ren, Science **8**, 4670 (2008).
[16]G. Joshi, X. Yan, H. Wang, W. Liu, G. Chen, and Z. F. Ren, Adv. Energy Mater. **1**, 643 (2011).
[17]X. Yan, G. Joshi,W. Liu, Y. Lan, H. Wang, S. Lee, J. W. Simonson, S. J. Poon, T. M. Tritt, G. Chen, and Z. F. Ren, Nano Lett. **11**, 556 (2011).
[18]J. Shiomi, K. Esfarjani, and G. Chen, Phys. Rev. B **84**, 104302 (2011).
[19]K. Esfarjani, G. Chen, and H. T. Stokes, Phys. Rev. B **84**, 085204 (2011).
[20]T. Shiga, J. Shiomi, J. Ma, O. Delaire, T. Radzynski, A. Lusakowski, K. Esfarjani, and G. Chen, Phys. Rev. B **85**, 155203 (2012).
[21]A. J. H. McGaughey and A. Jain, Appl. Phys. Lett. **100**, 061911 (2012).
[22]J. Garg, N. Bonini, B. Kozinsky, and N. Marzari, Phys. Rev. Lett. **106**, 045901 (2011).
[23]B. Abeles, Phys. Rev. **131**, 1906 (1963).
[24]H. Stohr and W. Klemm, Z. Anorg. Allg. Chem. **241**, 304 (1954).
[25]A. V. Ioffe and A. F. Ioffe, Izv. Akad. Nauk SSSR, Ser. Fiz. **20**, 65 (1956).
[26]I. Kudman, J. Mater. Sci. **7**, 1027 (1972).
[27]Y. K. Koh, C. J. Vineis, S. D. Calawa, M. P. Walsh, and D. G. Cahill, Appl. Phys. Lett. **94**, 153101 (2009).
[28]I. U. I. Ravich, B. A. Efimova, and I. A. Smirnov, *Semiconducting Lead Chalcogenides* (Plenum Press, New York, 1970).
[29]A. A. El-Sharkawy, A. M. Abou El-Azm, M. I. Kenawy, A. S. Hillal, and H. M. Abu-Basha, Int. J. Thermophys. **4**, 261 (1983).
[30]E. D. Devyatkova and I. A. Smirnov, Sov. Phys. Solid State **3**, 1675 (1962).
[31]T. Beechem, J. C. Duda, P. E. Hopkins, and P. M. Norris, Appl. Phys. Lett. **97**, 061907 (2010).
[32]A. S. Henry and G. Chen, J. Comput. Theor. Nanosci. **5**, 141 (2008).
[33]D. A. Broido, M. Malorny, G. Birner, N. Mingo, and D. A. Stewart, Appl. Phys. Lett. **91**, 231922 (2007).
[34]L. Sun and J. Y. Murthy, in *ASME Conf. Proc., San Francisco, CA HT2005-72200* (ASME, New York, NY, 2005).
[35]D. P. Sellan, J. E. Turney, A. J. H. McGaughey, and C. H. Amon, J Appl. Phys. **108**, 113524 (2010).
[36]Z. T. Tian, K. Esfarjani, J. Shiomi, A. S. Henry, and G. Chen, Appl. Phys. Lett. **99**, 053122 (2011).
[37]A. Ward and D. A. Broido, Phys. Rev. B **81**, 085205 (2010).
[38]O. Delaire, J. Ma, K. Marty, A. F. May, M. A. McGuire, M. H. Du, D. J. Singh, A. Podlesnyak, G. Ehlers, M. D. Lumsden, and B. C. Sales, Nat. Mater. **10**, 614 (2011).
[39]A. Debernardi, S. Baroni, and E. Molinari, Phys. Rev. Lett. **75**, 1819 (1995).
[40]S. Baroni, P. Giannozzi, and A. Testa, Phys. Rev. Lett. **58**, 1861 (1987).
[41]X. Gonze, Phys. Rev. A **52**, 1086 (1995).
[42]D. A. Broido, M. Malorny, G. Birner, N. Mingo, and D. A. Stewart, Appl. Phys. Lett. **91**, 231922 (2007).
[43]J. Garg, N. Bonini, and N. Marzari, Nano Lett. **11**, 5135 (2011).
[44]P. Giannozzi, S. Baroni, N. Bonini, M. Calandra, R. Car, C. Cavazzoni, D. Ceresoli, G. L. Chiarotti, M. Cococcioni, I. Dabo, A. Dal Corso, S. Fabris, G. Fratesi, S. de Gironcoli, R. Gebauer, U. Gerstmann, C. Gougoussis, A. Kokalj, M. Lazzeri, L. Martin-Samos, N. Marzari, F. Mauri, R. Mazzarello, S. Paolini, A. Pasquarello, L. Paulatto, C. Sbraccia, S. Scandolo, G. Sclauzero, A. P. Seitsonen, A. Smogunov, P. Umari, and R. M. Wentzcovitch, J. Phys.: Condens. Matter **21**, 395502 (2009).
[45]We used the pseudopotentials Pb.rel-pz-nc.UPF, Se.rel-pz-nc.UPF, and Te.rel-pz-nc.UPF from the PSlibrary of QEforge distribution [http://qe-forge.org/projects/pslibrary/].
[46]H. J. Monkhorst and J. D. Pack, Phys. Rev. B **13**, 5188 (1976).
[47]X. Gonze and J. P. Vigneron, Phys. Rev. B **39**, 13120 (1989).
[48]G. Deinzer, G. Birner, and D. Strauch, Phys. Rev. B **67**, 144304 (2003).
[49]A. A. Maradudin and A. E. Fein, Phys. Rev. **128**, 2589 (1962).
[50]R. A. Cowley, Rep. Prog. Phys. **31**, 123 (1968).
[51]G. P. Srivastava, *The Physics of Phonons* (Taylor and Francis, London, 1990).
[52]J. A. Reissland, *The Physics of Phonons* (Wiley, New York, 1973).
[53]C. Dames and G. Chen, in *Thermoelectrics Handbook: Macro to Nano*, edited by D. Rowe (CRC Press, Boca Raton, FL, 2005), 42-1.
[54]S. I. Tamura, Phys. Rev. B **27**, 858 (1983).
[55]P. R. Vijaraghavan, S. K. Sinha, and P. K. Iyengar, Proc. Nuc. Phys. and Solid State Symp. **16**, 208 (1973).
[56]W. Cochran, R. A. Cowley, G. Dolling, and M. M. Elcombe, Proc. R. Soc. London, Ser. A **293**, 433 (1966).
[57]J. An, A. Subedi, and D. J. Singh, Solid State Commun. **148**, 417 (2008).
[58]O. Kilian, G. Allan, and L. Wirtz, Phys. Rev. B **80**, 245208 (2009).
[59]Y. Zhang, X. Ke, C. Chen, J. Yang, and P. R. C. Kent, Phys. Rev. B **80**, 024304 (2009).
[60]P. Klemens, Proc. R. Soc. London A **208**, 108 (1951).